Geomechanics and Engineering, *Vol. 32, No. 5 (2023) 541-551*
https://doi.org/10.12989/gae.2023.32.5.541

Nonlinear snap-buckling and resonance of FG-GPLRC curved beams with different boundary conditions

Lei-Lei Gan and Gui-Lin She*

College of Mechanical and Vehicle Engineering, Chongqing University, Chongqing 400044, China

(*Received December 16, 2022, Revised February 10, 2023, Accepted February 15, 2023*)

Abstract. Snap-buckling is one of the main failure modes of structures, because it will lead to the reduction of structural bearing capacity, durability loss and even structural damage. Boundary condition plays an important role in the research of engineering mechanics. Further discussion on the boundary conditions problems will help to analyze the dynamic and static behavior of structures more accurately. Therefore, in order to understand the dynamic and static behavior of curved beams more comprehensively, this paper mainly studies the nonlinear snap-through buckling and forced vibration characteristics of functionally graded graphene reinforced composites (FG-GPLRCs) curved beams with two different boundary conditions (including clamped-hinged and hinged-hinged) using Euler-Bernoulli beam theory (E-BBT). In addition, the effects of the curved beam radius, the GLPs distributions, number of GLPs layers, the mass fraction of GLPs and elastic foundation parameters on the nonlinear snap-through buckling and forced vibration behavior are discussed respectively.

Keywords: boundary condition; curved beams; resonance; snap-through buckling; two-step perturbation method

1. Introduction

Elastic foundation is relative to rigid foundation such as rubble foundation. Elastic foundation can bear certain bending moment and deformation. Because of its unique engineering value and research significance, many researchers have carried out research on it. For example: Chen *et al.* (2022) employed the Newmark method to study the steady response of an infinite beam resting on a tensionless visco-elastic foundation under uniform motion. Pham *et al.* (2022) used the finite element method (FEM) to research the hygrothermal vibration characteristics of biaxial functionally graded (FG) porous curved beams on a two-layer elastic foundation. Pham *et al.* (2022) adopted the high order shear deformation beam theory (HOSDBT) to illustrate the dynamic instability of magnetic embedded FG porous nano-beams. Xiong *et al.* (2022) discussed the longitudinal displacement of simplified tunnel model based on elastic foundation beam using the combination of isogeometric analysis. Daikh *et al.* (2022) developed a three-dimensional analytical plate theory based on Winkler/Pasternak elastic foundation to investigate the bending behavior of FG plate under different boundary conditions. The tracking control and active vibration suppression of a rigid elastic hybrid vibration mobile system with nonlinear elastic foundation are considered by Homaeinezhad and Gavari (2022). Abumandour *et al.* (2022) proposed the E-BBT to deliberate the bending behavior of nano beams placed on two linear elastic bases under different forces. Mohamed *et al.* (2022), Qiao *et al.* (2022) discussed the nonlinear bending and penetration instability of composite beams with helical orientation on three parameter elastic foundation. Employing HOSDBT, Chaabani *et al.* (2022) analyzed the buckling behavior of FG porous sandwich plates on Winkler Pasternak elastic foundation. Chinnapandi *et al.* (2022) explored the vibration acoustic behavior of FG beams on elastic foundation under external loads by the FEM.

With the development of engineering construction, it is particularly important to study the dynamic and static mechanics of curved structure. Curved structure is an important structural form in engineering applications, which is widely used in aerospace, materials science and engineering and bridge construction fields, and has high research value, there are a lot of literatures on curved structure. Deng *et al.* (2023) used the Lagrangian-Euler formula to study the geometrically nonlinear dynamic analysis of a plane bending elastic beam under moving loads. Zhai *et al.* (2023) came up with a nonlinear dynamic model to study the connection structure of two micro curved beams. Wang *et al.* (2023) employed the Halpin Tsai method to analyze the energy absorption capacity of sandwich curved beam structures. Chen *et al.* (2023) designed the compliant planar parallelogram mechanism based on 8 flexible initial bending beams to realize the high-precision translation of the mechanism. Melchiorre *et al.* (2023) solved the static and kinematic equations of curved beams by alternative analytical and numerical methods. Kallannavar and Kattimani (2023) used the first order shear deformation theory (FOSDT) to illustrate the effects of temperature and porosity on the vibration response of hyperbolic inclined sandwich composite shells. Shahmohammadi *et al.* (2023) utilized the FOSDT to discuss the geometric nonlinearity and size dependent response of sandwich curved microplate. Tornabene *et al.*

*Corresponding author, Distinguished Professor
E-mail: sheguilin@cqu.edu.cn

ISSN: 2005-307X (Print), 2092-6219 (Online)

(2023) advanced the layered generalized model for the linear static analysis of hyperbolic shells subjected to general boundary conditions. Pham *et al.* (2022) researched the hygrothermal vibration characteristics of a two-way FG porous curved beam on a two-layer elastic foundation using the FEM. Through modeling, Li and his partners (2022) analyzed the nonlinear dynamic behavior of FG-GPLRCs curved sandwich beams. Ermis *et al.* (2022) used the FEM to explain the free vibration characteristics of FG curved beam on Pasternak foundation. Pham *et al.* (2022) applied the FOSDT to illustrate the free vibration of doubly curved shells with FG material panels and honeycomb core layers. Tornabene *et al.* (2022) utilized the HOSDBT to analyze the free vibration characteristics of laminated hyperbolic shells under common boundary condition. Al-Furjan *et al.* (2022) exploited the differential cube method to discuss the energy absorption and vibration behavior of FG perforated curved conical plate. Amir *et al.* (2022) employed the FEM to study the random vibration behavior of honeycomb curved plates. Based on the FOSDT, Hu *et al.* (2022) analyzed the free vibration of bending plates with variable thickness and curvature. Van Long *et al.* (2022) applied the FOSDT to analyze the nonlinear dynamic behavior of FGM doubly curved shell under the action of underwater explosion. Jiang *et al.* (2022) solved the problem of vibration response of FG graphene nano sheet reinforced composite curved shells. Esmaeili and Kiani (2022) used the FOSDT to analyze the vibration behavior of graphene sheet reinforced composite curved shell. Numerical analysis is carried out to discuss the fracture phenomenon of the curved shell under vertex loading by Huang *et al.* (2022). Gao *et al.* (2020) applied the strain gradient theory to investigate the snap-buckling behavior of FG-GPLRCs curved nano-beams with geometric defects. Tung (2018) employed the FOSDT to study the nonlinear dynamic behavior of doubly curved FG material sandwich plates. Babaei and his partners published a lot of papers (Babaei 2021, Babaei 2022a, b, Babaei and Eslami 2021a, 2022b, Babaei *et al.* 2019a, b, c, d, e, Babaei *et al.* 2018a, b, c), in which they systematically studied the static and dynamic behavior of curved beam and curved tube structures. Eltaher and his co-workers (Alazwari *et al.* 2021, Assie *et al.* 2023, Basha *et al.* 2022, Chinnapandi *et al.* 2022, Daikh *et al.* 2022, Eltaher *et al.* 2019, Hendi *et al.* 2022, Mohamed *et al.* 2021, Mohamed *et al.* 2022) made great efforts to illustrate the importance of the snap-through and buckling of imperfect structures. Over the years, She and his collaborators have published a series of works (Zhao *et al.* 2022a, b, Zhang *et al.* 2021, Zhang *et al.* 2022, Zhang *et al.* 2023a, b, Zhang and She 2022, Zhang and She 2023a, Zhang and She 2023b, Xu and She 2022, She 2020, She 2021, She and Ding 2023, She *et al.* 2022, She and Li 2022, She *et al.* 2021, Lu *et al.* 2021, Chen *et al.* 2022a, 2022b, Ding and She 2021, Ding *et al.* 2022a, b), but none of them examined snap-buckling and resonance of curved beams with simply supported and one edge simply supported and one edge clamped.

By consulting the literatures, we can find that the literatures on nonlinear snap-through bucking and resonance of curved beams is very limited. In the early stage of the research work, the influence of C-C boundary condit1ion on the dynamic behavior of curved beams is considered. On the basis of this work (Zhang *et al.* 2022b), we will carry out the current work, in which two kinds of boundary conditions (include C-H and H-H) are considered. This study provides a significant reference value for the subsequent research on the dynamic behavior of curved structures under different boundary conditions.

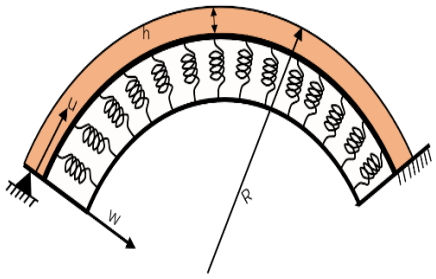

Fig. 1 A curved beam with two different boundary conditions

2. Problem formulation

Because the only difference between this paper and our previous papers is that we have considered the new boundary conditions. In our previous research work, we only studied the fixed boundary conditions, while in this paper, we considered the other two boundary conditions. Namely: simply supported boundary and one end simply supported and one end clamped. Therefore, other factors are the same. That is, the length, thickness and radius of curvature of FG-GPLRCs curved beams are expressed by L, h, and R respectively. Similarly, we use the micromechanical model to express the elastic modulus, density and Poisson's ratio of the beam. For specific formulas, refer to the literature (Zhang *et al*. 2022, Malikan *et al.* 2019, 2022). Similarly, we consider four different GPLs distribution types, including the following expressions (Zhang *et al*. 2022)

$$g_{GPL}^{(k)}=\begin{cases} g, & (\mathrm{UD}) \\ 4g\left(\dfrac{N+1}{2}-\left|k-\dfrac{N+1}{2}\right|\right)\Big/(2+N), & (\mathrm{FG\text{-}O}) \\ 4g\left(\dfrac{1}{2}+\left|k-\dfrac{N_L+1}{2}\right|\right)\Big/(2+N), & (\mathrm{FG\text{-}X}) \\ 2kg/(2+N), & (\mathrm{FG\text{-}A}) \end{cases} \tag{1}$$

In which, g is the mass fraction of GPLs, N is the total layer of GPLs, UD, FG-O, FG-X and FG-A are the types of GLPs distribution. If the shell model is used, it will greatly increase the difficulty of calculation. Therefore, for the sake of convenience, the Euler beam theory is adopted in this paper, because both theory and experiment show that the Euler beam model is appropriate as long as the ratio of length to thickness is greater than five. Similarly, we use the

Euler beam model to express the displacement field and neglect the thermal effect, the following dimensionless vibration equation can be derived (Zhang *et al*. 2022)

$$\begin{aligned}&\xi_1\frac{\partial^4 W}{\partial X^4}+K_1W-K_2\frac{\partial^2 W}{\partial X^2}+\xi_{10}\frac{\partial^2 W}{\partial \tau^2}+\xi_{11}\frac{\partial^4 W}{\partial X^2\partial \tau^2}\\&-\int_0^{\pi}\left[\frac{\pi\xi_0}{2}\left(\frac{\partial W}{\partial X}\right)^2-\pi\xi_2\left(\frac{\partial^2 W}{\partial X^2}\right)-R\pi\xi W\right]dX\\&\times\left(\frac{\partial^2 W}{\partial X^2}+r\right)=\lambda_q.\end{aligned}\tag{2}$$

3. The solution of simply supported boundary and one end simply supported and one end fixed

According to the two-step perturbation method (Babaei 2021, Babaei 2022a, b, Babaei and Eslami 2021a, 2022b, Zhang *et al*. 2022), the first order to third order perturbation equation without thermal effect has the following expressions

$$\begin{aligned}&O\left(\varepsilon^1\right):\xi_1\frac{\partial^4 W_1}{\partial X^4}+K_1W_1-K_2\frac{\partial^2 W_1}{\partial X^2}+\xi_{10}\frac{\partial^2 W_1}{\partial \tau^2}\\&+\xi_{11}\frac{\partial^4 W_1}{\partial X^2\partial \tau^2}+r\int_0^{\pi}\left[\pi\xi_2\frac{\partial^2 W_1}{\partial X^2}+r\pi\xi_0W_1\right]dx=\lambda_1^{(1)},\\&O\left(\varepsilon^2\right):\xi_1\frac{\partial^4 W_2}{\partial X^4}+K_1W_2-K_2\frac{\partial^2 W_2}{\partial X^2}+\xi_{10}\frac{\partial^2 W_2}{\partial \tau^2}\\&+\xi_{11}\frac{\partial^4 W_2}{\partial X^2\partial \tau^2}+r\int_0^{\pi}\left[\pi\xi_2\frac{\partial^2 W_2}{\partial X^2}+r\pi\xi_0W_2\right]dx\\&+\int_0^{\pi}\left[\pi\xi_2\left(\frac{\partial^2 W_1}{\partial X^2}\right)+r\pi\xi_0W_1\right]dx\cdot\frac{\partial^2 W_1}{\partial X^2}\\&-r\int_0^{\pi}\frac{\pi\xi_0}{2}\left(\frac{\partial^2 W_1}{\partial X^2}\right)^2dx=\lambda_2^{(1)},\end{aligned}\tag{3}$$

$$\begin{aligned}&O\left(\varepsilon^3\right):\xi_1\frac{\partial^4 W_3}{\partial X^4}+K_1W_2-K_2\frac{\partial^2 W_3}{\partial X^2}+\xi_{10}\frac{\partial^2 W_3}{\partial \tau^2}\\&+\xi_{11}\frac{\partial^4 W_3}{\partial X^2\partial \tau^2}+r\int_0^{\pi}\left[\pi\xi_2\frac{\partial^2 W_3}{\partial X^2}+r\pi\xi_0W_3\right]dx\\&+\int_0^{\pi}\left[\pi\xi_2\left(\frac{\partial^2 W_3}{\partial X^2}\right)+r\pi\xi_0W_3\right]dx\cdot\frac{\partial^2 W_3}{\partial X^2}\\&-r\int_0^{\pi}\frac{\pi\xi_0}{2}\left(\frac{\partial^2 W_3}{\partial X^2}\right)^2dx-\int_0^{\pi}\frac{\pi\xi_0}{2}\left(\frac{\partial W_1}{\partial X}\right)^2dx\cdot\frac{\partial^2 W_1}{\partial X^2}=\lambda_3^{(1)}.\end{aligned}$$

Case 1: For hinged-hinged (H-H) ends,

Assuming that Eq. (3) has a solution in the following form (Ding *et al*. 2022a)

$$\begin{cases}W_1(X,\tau)=A_{10}^{(1)}(\tau)\sin\left(X\right)\\W_2(X,\tau)=A_{20}^{(1)}(\tau)\sin\left(2X\right)\\W_3(X,\tau)=A_{30}^{(1)}(\tau)\sin\left(3X\right)\end{cases}\tag{4}$$

in which, $A_{10}^{(1)}(\tau),A_{20}^{(1)}(\tau),\text{and }A_{30}^{(1)}(\tau)$ represent small perturbation parameters. Substituting Eq. (4) into Eq. (3) leads to

$$\begin{aligned}&\lambda_1^{(1)}=\left(\xi_{10}-\xi_{11}\right)\frac{\partial^2 A_{10}^{(1)}}{\partial \tau^2}\sin X\\&+\left(\xi_1\sin X+K_1\sin X+K_2\sin X-2\pi r\xi_2+2\pi r^2\xi_0\right)A_{10}^{(1)},\\&\lambda_2^{(2)}=\left(A_{20}^{(1)}\right)^2\left[2\pi\xi_2\sin X-2r\pi\xi_0\sin X-\frac{\pi^2}{4}r\xi_0\right],\\&\lambda_3^{(3)}=\frac{\pi^2\xi_0}{4}\left(A_{10}^{(1)}\right)^3\sin X.\end{aligned}\tag{5}$$

Therefore, for simply supported boundary, the relationship between load and amplitude is as follows

$$\begin{aligned}&\lambda_q\left(X,\tau,\varepsilon\right)=\lambda_{q0}\cos\left(\Omega\tau\right)\\&=\lambda_1^{(1)}+\lambda_2^{(1)}+\lambda_3^{(1)}+O\left(\varepsilon^4\right)=\left(\xi_{10}-\xi_{11}\right)\frac{\partial^2 A_{10}^{(1)}}{\partial \tau^2}\sin X\\&+\left(\xi_1\sin X+K_1\sin X+K_2\sin X-2\pi r\xi_2+2\pi r^2\xi_0\right)A_{10}^{(1)}\\&+\left(A_{10}^{(1)}\right)^2\left[2\pi\xi_2\sin X-2r\pi\xi_0\sin X-\frac{\pi^2}{4}r\xi_0\right]+\frac{\pi^2\xi_0}{4}\left(A_{10}^{(1)}\right)^3\sin X\end{aligned}\tag{6}$$

Case 2: For clamped-hinged (C-H) ends,

At this time, we use the displacement shape function in the following form (Ding *et al*. 2022a)

$$\begin{cases}W_1(X,\tau)=A_{10}^{(1)}(\tau)\left(\cos\frac{X}{2}-\cos\frac{3X}{2}\right)\\W_2(X,\tau)=A_{20}^{(2)}(\tau)\left(\cos\frac{3X}{2}-\cos\frac{5X}{2}\right)\\W_3(X,\tau)=A_{30}^{(3)}(\tau)\left(\cos\frac{5X}{2}-\cos\frac{7X}{2}\right)\end{cases}\tag{7}$$

Substituting Eq. (7) into Eq. (3) leads to

$$\begin{aligned}\lambda_1^{(3)}&=A_{10}^{(1)}\left[\begin{array}{l}\xi_1\left(\frac{1}{16}\cos\frac{X}{2}-\frac{16}{81}\cos\frac{3X}{2}\right)+K_1\left(-\cos\frac{3X}{2}+\cos\frac{X}{2}\right)\\-K_2\left(\frac{9}{4}\cos\frac{3X}{2}-\frac{1}{4}\cos\frac{X}{2}\right)-2r\pi\xi_2+\frac{8}{3}r^2\pi\xi_0\end{array}\right]\\&+\left[\xi_{10}\left(\cos\frac{X}{2}-\cos\frac{3X}{2}\right)+\xi_{11}\left(\frac{9}{4}\cos\frac{3X}{2}-\frac{1}{4}\cos\frac{X}{2}\right)\right]\frac{\partial^2 A_{10}^{(1)}}{\partial \tau^2},\\\lambda_2^{(3)}&=\left[\begin{array}{l}-\frac{5}{8}\pi^2\xi_0-2\pi\xi_2\left(\frac{9}{4}\cos\frac{3X}{2}-\frac{1}{4}\pi\gamma_2\cos\frac{X}{2}\right)\\+\frac{8}{3}\pi r\gamma_0\left(\frac{9}{4}\cos\frac{3X}{2}-\frac{1}{4}\pi\gamma_2\cos\frac{X}{2}\right)\end{array}\right]\left(A_{10}^{(1)}\right)^2,\\\lambda_3^{(3)}&=\left[-\frac{5}{8}\pi^2\gamma_0\left(\frac{9}{4}\cos\frac{3X}{2}-\frac{1}{4}\pi\gamma_2\cos\frac{X}{2}\right)\right]\left(A_{10}^{(1)}\right)^3.\end{aligned}\tag{8}$$

$$\begin{aligned}&\lambda_q\left(X,\tau,\varepsilon\right)=\lambda_{q0}\cos\left(\Omega\tau\right)=\lambda_1^{(2)}+\lambda_2^{(2)}+\lambda_3^{(2)}+O\left(\varepsilon^4\right)\\&=A_{10}^{(1)}\left[\begin{array}{l}\xi_1\left(\frac{1}{16}\cos\frac{X}{2}-\frac{16}{81}\cos\frac{3X}{2}\right)+K_1\left(-\cos\frac{3X}{2}+\cos\frac{X}{2}\right)\\-K_2\left(\frac{9}{4}\cos\frac{3X}{2}-\frac{1}{4}\cos\frac{X}{2}\right)-2r\pi\xi_2+\frac{8}{3}r^2\pi\xi_0\end{array}\right]\\&+\left[\xi_{10}\left(\cos\frac{X}{2}-\cos\frac{3X}{2}\right)+\xi_{11}\left(\frac{9}{4}\cos\frac{3X}{2}-\frac{1}{4}\cos\frac{X}{2}\right)\right]\frac{\partial^2 A_{10}^{(1)}}{\partial \tau^2}\\&+\left[\begin{array}{l}-\frac{5}{8}\pi^2\xi_0-2\pi\xi_2\left(\frac{9}{4}\cos\frac{3X}{2}-\frac{1}{4}\pi\gamma_2\cos\frac{X}{2}\right)\\+\frac{8}{3}\pi r\gamma_0\left(\frac{9}{4}\cos\frac{3X}{2}-\frac{1}{4}\pi\gamma_2\cos\frac{X}{2}\right)\end{array}\right]\left(A_{10}^{(1)}\right)^2\\&+\left[-\frac{5}{8}\pi^2\gamma_0\left(\frac{9}{4}\cos\frac{3X}{2}-\frac{1}{4}\pi\gamma_2\cos\frac{X}{2}\right)\right]\left(A_{10}^{(1)}\right)^3\end{aligned}\tag{9}$$

For Eq. (9), the following Duffing equation can be obtained by Galerkin method

$$\begin{cases} \lambda_{q0}\cos(\Omega\tau)=\dfrac{\pi}{4}(\xi_{10}-\xi_{11})\dfrac{\partial^2 A_{10}^{(1)}}{\partial\tau^2} \\ +\dfrac{\pi}{4}\left(8\xi_0 r^2-8\xi_2 r^2+\xi_1+K_1+K_2\right)A_{10}^{(1)} \\ +\left(\xi_2 r^2-\dfrac{3}{2}\xi_0 r\pi^2\right)\left(A_{10}^{(1)}\right)^2+\left(A_{10}^{(1)}\right)^3\dfrac{\pi^2\xi_0}{8}, \quad (\text{for H-H ends}) \\ \lambda_{q0}\cos(\Omega\tau) \\ =\dfrac{3}{8}\pi\left[\dfrac{41}{16}\xi_1+K_1+\dfrac{5}{4}K_2-\dfrac{16}{3}r\xi_2+\dfrac{64}{9}r^2\xi_0\right]A_{10}^{(1)} \\ +\dfrac{3\pi}{32}(4\xi_{10}-5\xi_{11})\dfrac{\partial^2 A_{10}^{(1)}}{\partial\tau^2} \\ +\dfrac{3}{8}\left(\dfrac{5}{2}\pi^2\xi_2-5\pi^2 r\xi_0\right)\left(A_{10}^{(1)}\right)^2+\dfrac{75}{256}\pi^3\xi_0\left(A_{10}^{(1)}\right)^3, \quad (\text{for C-H ends}) \end{cases} \tag{10}$$

In this case, the Modified LP method (Ding *et al*. 2022a) can be used to obtain the expression of the amplitude frequency response relationship of the forced vibration. For static problems, we ignore the inertia term. At this time, the relationship between load and displacement can be expressed as

$$\lambda_{q0}=\begin{cases} \dfrac{\pi}{4}\left(8\xi_0 r^2-8\xi_2 r^2+\xi_1+K_1+K_2\right)A_{10}^{(1)} \\ +\left(\xi_2 r^2-\dfrac{3}{2}\xi_0 r\pi^2\right)\left(A_{10}^{(1)}\right)^2+\left(A_{10}^{(1)}\right)^3\dfrac{\pi^2\xi_0}{8}, \\ (\text{for H-H ends}) \\ \dfrac{3}{8}\pi\left[\dfrac{41}{16}\xi_1+K_1+\dfrac{5}{4}K_2-\dfrac{16}{3}r\xi_2+\dfrac{64}{9}r^2\xi_0\right]A_{10}^{(1)} \\ +\dfrac{3}{8}\left(\dfrac{5}{2}\pi^2\xi_2-5\pi^2 r\xi_0\right)\left(A_{10}^{(1)}\right)^2 \\ +\dfrac{75}{256}\pi^3\xi_0\left(A_{10}^{(1)}\right)^3, \quad (\text{for C-H ends}) \end{cases} \tag{11}$$

4. Numerical calculation and discussion

In Fig. 2, the influence of $\lambda = L^2/(Rh)$ is examined. In this figure and the subsequent forced vibration response curves, the curve bent to the left represents the performance of the soft-spring, while the curve bent to the right represents the performance of the hard-spring. From the figure, we can see that the λ has an important influence on the forced vibration behavior of curved beams, whether C-H curved beams or H-H curved beams. And the resonance frequency of C-H curved beam and H-H curved beam decrease with the decrease of λ, that is, when λ is very small (λ= 5), the resonance phenomenon occurs first. In addition, we can also observe that the maximum amplitude of H-H curved beam is greater than that of C-H curved beam. What is more, the forced vibration response curves of C-H and H-H curved beams are characterized by soft-spring.

Fig. 3 studies the influence of GPLs distribution type, and considers the influence of four distribution types on the

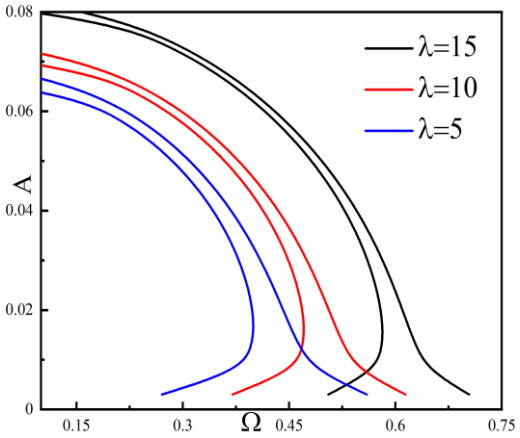

(a) FG-A C-H

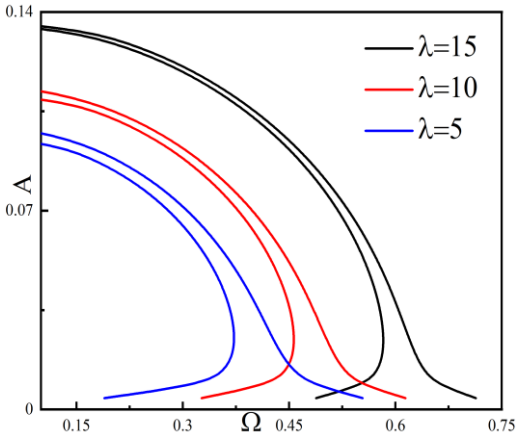

(b) FG-A H-H

Fig. 2 Ω-A for radius of curved beam at λ_q =0.04, N=9, g=0.2, L=0.5, h=0.05, k1=0, k2=8e6, r=20*h

resonant behavior of curved beams. It is obvious that GPLs distribution type has a significant effect. In particular, under the UD distribution type, C-H and H-H curved beams have the largest vibration frequency, followed by FG-O, FG-X and FG-A, this is because different materials distribution will lead to different physical and mechanical properties of the structure. Finally, we can see that under the four different material distribution types, the forced vibration curves of C-H and H-H curved beams all bend to the right, showing the performance of hard-spring, and the more backward the resonance position of the curve, the less obvious the phenomenon of hard-spring.

Fig. 4 shows the influence of GPLs mass fraction on the forced vibration characteristics of curved beams. It is not difficult to find that under the action of different GPLs mass fraction, the change trend of forced vibration response curves of C-H and H-H curved beams are highly consistent, and the resonance position of C-H and H-H curved beams will be delayed as GPLs mass fraction goes up, thus, when g=0.2, C-H and H-H curved beams have the largest vibration position. Furthermore, we can also notice that the forced vibration response curves of C-H and H-H curved beams bend towards the high frequency direction, and this phenomenon is more obvious with the increase of the mass fraction of GPLs.

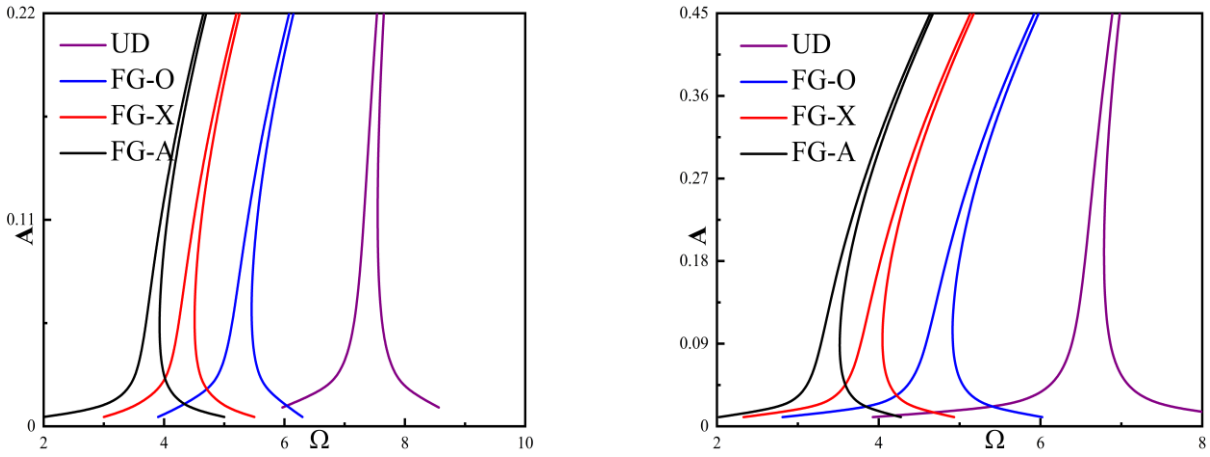

(a) FG-A C-H (b) FG-A H-H

Fig. 3 Ω-A for types of GLPs distribution at r=80*h, λ_q =20, N=9, g = 0.55, L/h=10, k1=5e9, k2=5e9 λ_q =0.6, N=9, L=0.5, h=0.05, k1=4e10, k2=4e9, r=20*h

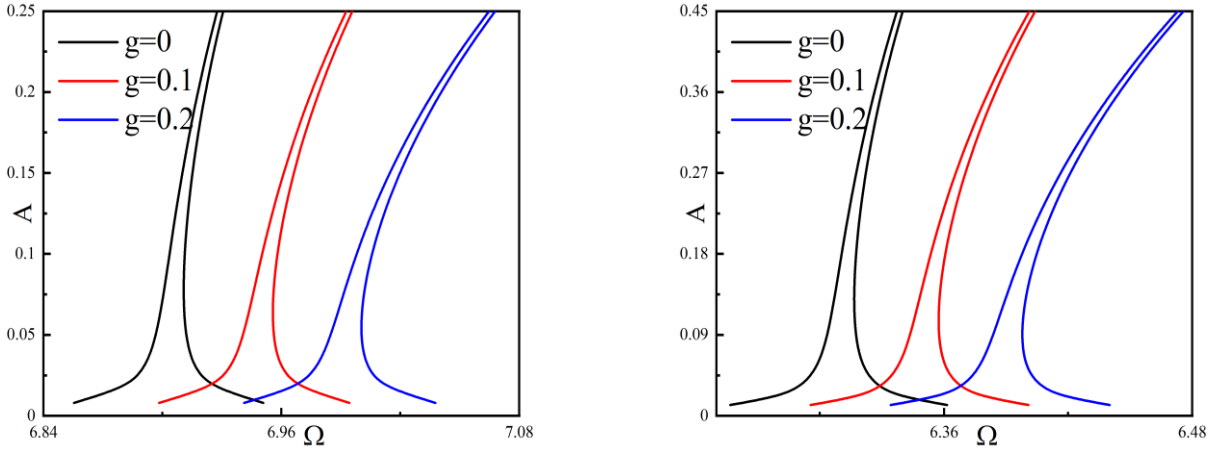

(a) FG-A C-H (b) FG-A H-H

Fig. 4 Ω-A for mass fraction of GLPs g at λ_q =0.6, N=9, L=0.5, h=0.05, k1=4e10, k2=4e9, r=20*h

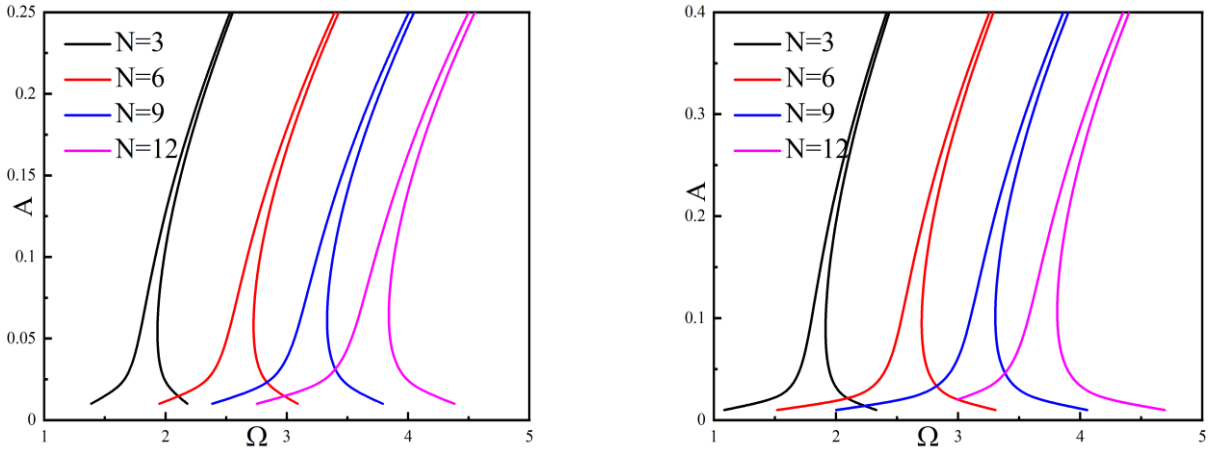

(a) FG-A C-H (b) FG-A H-H

Fig. 5 Ω-A for GLPs layers at λ_q =0.5, N=9, L=0.5, h=0.05, k1=5e9, k2=0, r=20*h, g_{GNP}=0.4

Fig. 5 analyzes the influence of the number of layers of GPLs on the amplitude frequency response curve of curved beams. From the figure, we can see that when the number of GPLs is three, the C-H and H-H curved beams have the

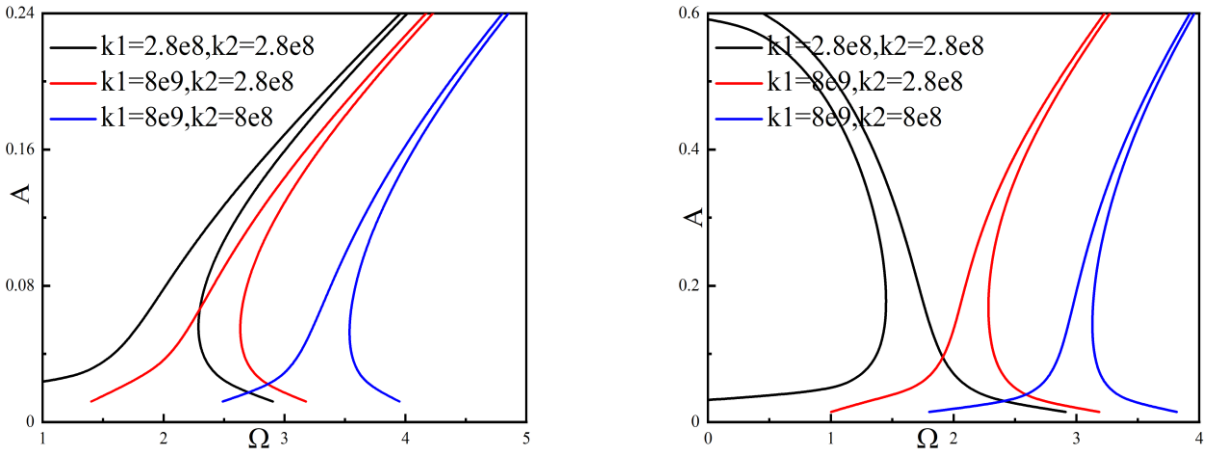

(a) FG-A C-H (b) FG-A H-H

Fig. 6 Ω-A for elastic foundations at λ_q =6, N=9, L=0.5, h=0.05, r=20*h, g_{GNP}=0.6

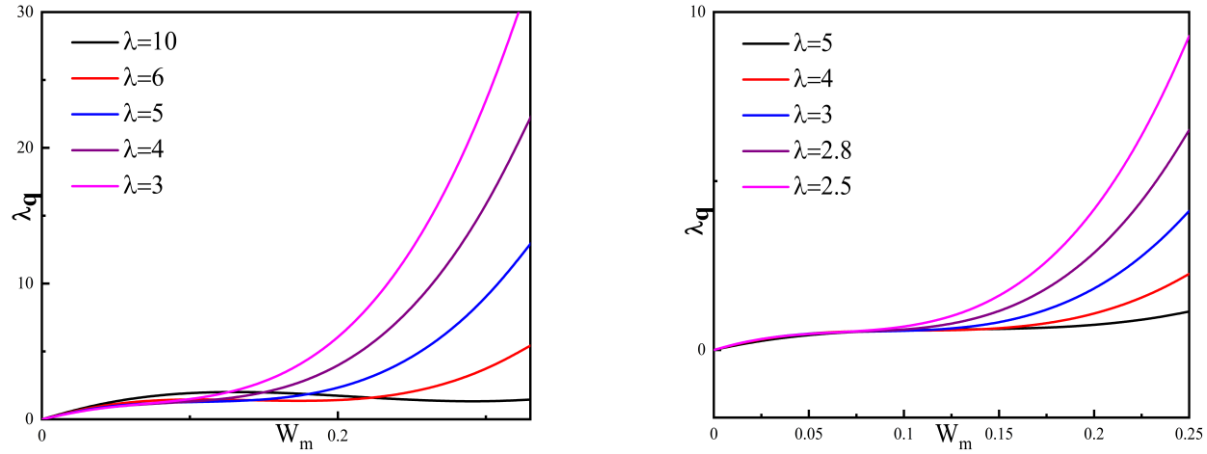

(a) FG-A C-H (b) FG-A H-H

Fig. 7 A- λ_q for the radius of curved beam (a) at L/h=10, N=9, k1=3e8, k2=1e5, g=0.01 and (b) at L/h=10, N=9, k1=1e8, k2=5e7, g=0.01

minimum resonance position. With the increase of the number of layers, the resonance position will be delayed. When the GPLs layers increase to a certain value (N=12), C-H and H-H curved beams have the largest resonance position. The main reason for this phenomenon is that the number of layers of material will seriously affect the stiffness characteristics of the structure, so as to affect the resonance behavior of the structure. Exactly, the hard-spring characteristics of C-H and H-H curved beams will not be affected by the number of GPLs.

Fig. 6 depicts the effect of three different elastic foundations. As shown, as K1 and K2 increase respectively, the resonance frequency of C-H and H-H curved beams also increase, that is, the resonance position is delayed. The difference is that, compared with the forced vibration curve of H-H curved beam, the forced vibration curve of C-H curved beam bends to the right, showing the nature of hard-spring. However, for H-H curved beams, when the values of K1 and K2 are the smallest, the forced vibration curve of H-H curved beams bends to the left. It can be clearly seen that with the increase of K1 and K2, the H-H curved beam will change from soft-spring property to hard-spring property.

Fig. 7 studies the influence of $\lambda=L^2/(Rh)$ on the nonlinear buckling response of curved beams. From the figure, we can see that the nonlinear buckling behavior of C-H and H-H curved beams become less and less obvious with the increase of λ. This is because the larger the λ is, the smaller the radius of curvature of the curved beam is, the better the stability of the structure is. On the contrary, the smaller the λ is, the larger the radius of curvature is, the worse the stability of the structure is, and the more likely the nonlinear buckling phenomenon occurs. This is because the radius of curvature will seriously affect the stability of the structure.

Fig. 8 studies the effect of GPLs distribution type on the deflection-loading curve of curved beam. As shown in the figure, with the increase of the deflection, the loading also increases, at this time, the loading is proportional to the deflection. But when exceeding a certain limit point (this limit point is called the upper buckling loading), the loading will decrease with the increase of the deflection until reaching the second limit point (lower buckling loading),

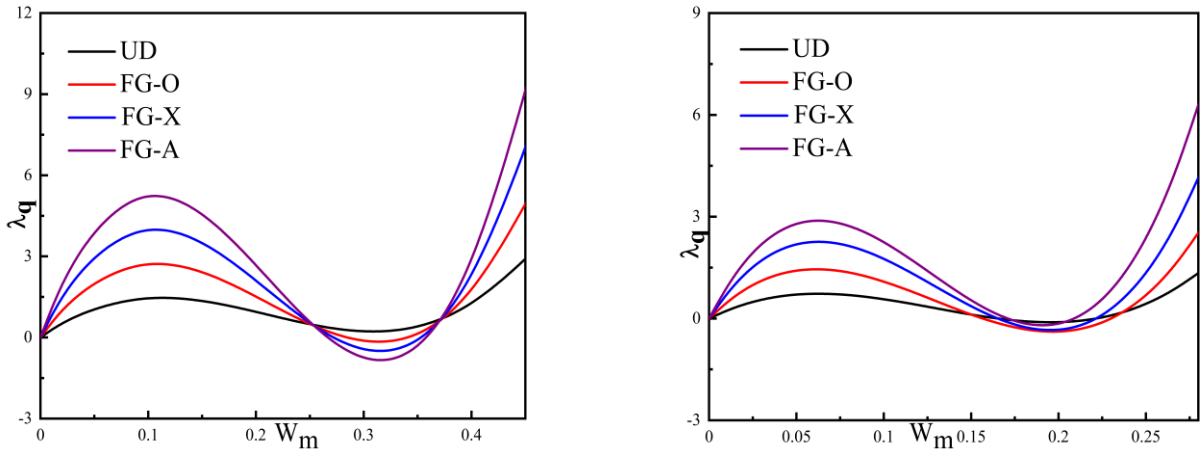

(a) FG-A C-H (b) FG-A H-H

Fig. 8 A- λ_q for GLPs distribution of the curved beams: (a) at r=10*h, L/h=10, N=9, k1=0, k2=2e6, g=0.01 and (b) at r=25*h, L/h=10, N=9, k1=0, k2=9e7, g=0.1

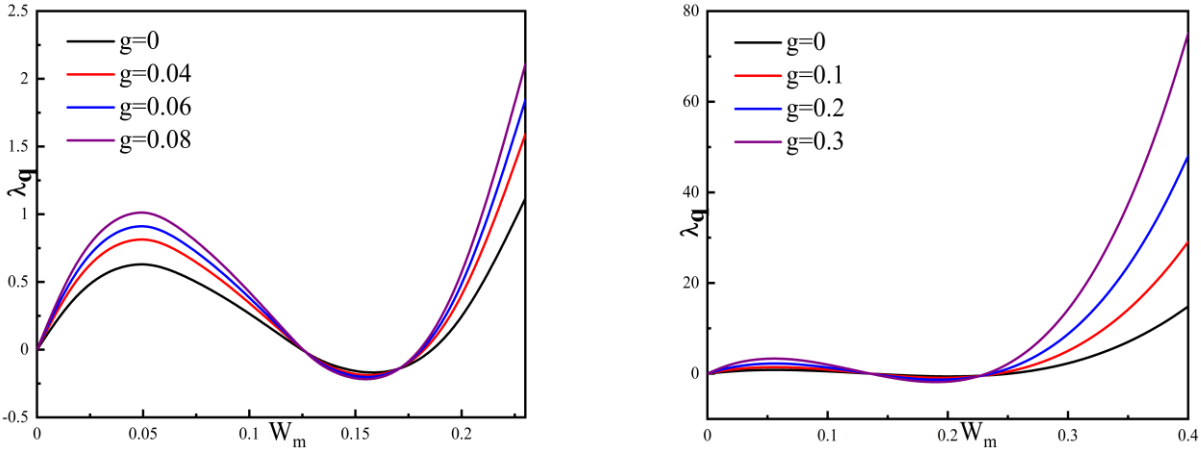

(a) FG-A C-H (b) FG-A H-H

Fig. 9 A- λ_q for mass fraction of GLPs of the curved beam (a) at r=20*h, L/h=20, N=9, k1=0, k2=0 and (b) at r=20*h, L/h=20, N=9, k1=0, k2=2e7

the loading will increase again with the increase of the deflection. This phenomenon is called "jump buckling" which refers to that the structure has two or more equilibrium positions under a certain loading. In addition, we also call the D-value between the upper buckling loading and the lower buckling loading "buckling strength". It can be seen from the Fig. 8 that both C-H and H-H curved beams have obvious jump buckling, especially under the FG-A distribution, C-H and H-H curved beams have the largest buckling strength, followed by FG-X, FG-O and UD.

Fig. 9 researches the impact of GPLs mass fraction on the snap-buckling behavior of curved beam. By comparing Figs. 10(a) and 10(b), we can see that the mass fraction of GPLs has the same effect on the snap-buckling behavior of C-H and H-H curved beams. That is, when g=0, both have the minimum buckling strength, and with the increase of GPLs mass fraction, the buckling strength of C-H and H-H curved beams also increase. The reason for this phenomenon is that the increase of GPLs mass fraction will enhance the structural stiffness.

Fig. 10 discusses the influence of different layers of GPLs on the deflection-loading curve of curved beam. We can see that the buckling strength of curved beam changes significantly with the number of GPLs changes. In other words, the buckling strength of C-H and H-H curved beams will increase as the number of GPLs increase, and when N=12, there is the maximum buckling strength, followed by N=9, N=6 and N=3. Therefore, we can know that the number of GPLs has a significant impact.

Fig. 11 illustrates the effect of elastic foundation. Three kinds of elastic foundations are considered. It is not difficult to see that the deflection-loading response curves of C-H and H-H curved beams have the same change trend under three different elastic foundations. As we have seen, when there is no elastic foundation (K1=K2=0), the deflection-loading curves of C-H and H-H curved beams are located at the bottom of the whole. With the addition of elastic foundation, the C-H and H-H deflection load curves will gradually move upward. When the elastic foundation

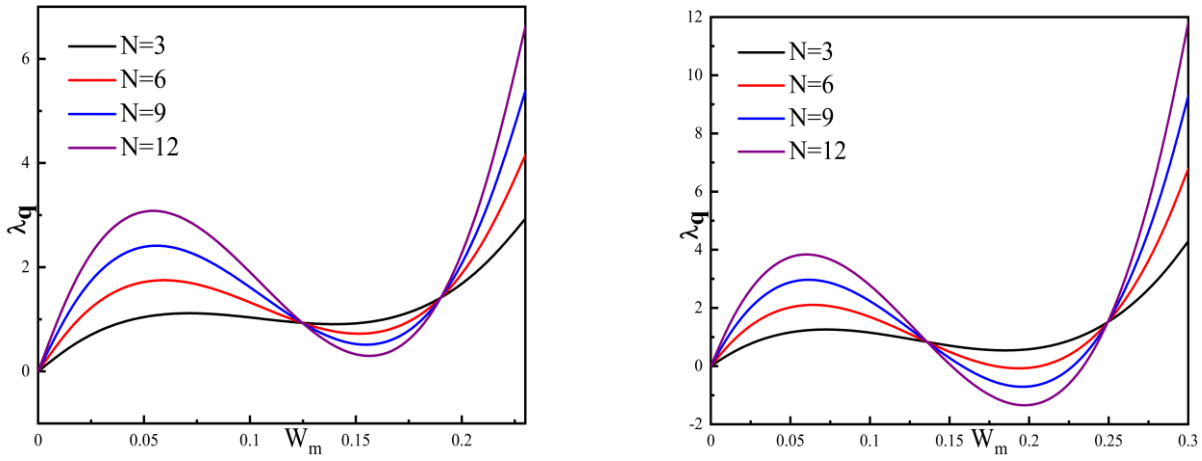

(a) FG-A C-H (b) FG-A H-H

Fig. 10 A- λ_q for GLPs layers of the curved beam at r=20*h, L/h=20, N=9, k1=0, k2=2e6, g=0.01

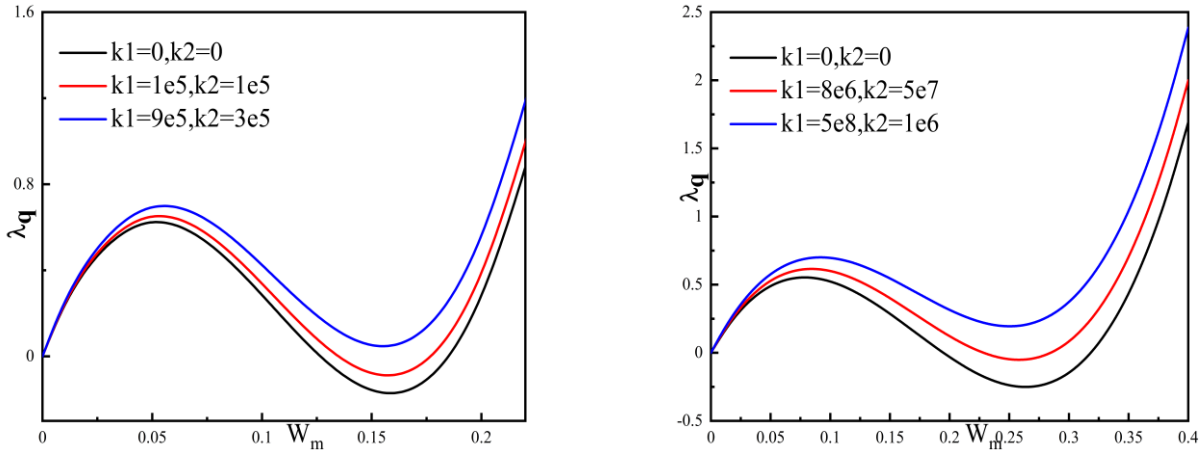

(a) FG-A C-H (b) FG-A H-H

Fig. 11 A- λ_q for elastic foundations of the curved beam at r=15*h, g = 0.01, L/h=20, N=9

increases to a certain value (K1=9e5, K2=3e5 for C-H curved beam; K1=5e8, K2=1e6 for H-H curved beam), there is a maximum limit position. This is because the elastic foundation has a very important influence on the static performance of the structure.

5. Conclusions

Through numerical analysis and theoretical research, the main conclusions can be summarized as follows:

(1) The radius has the same effect on the forced vibration and snap-bucking behavior of C-H and H-H curved beams. That is, when the radius decreases, the resonance position of C-H and H-H curved beams is delayed, and the snap-buckling phenomenon is more difficult to occur.

(2) Under certain external factors, the dynamic and static behaviors of curved beams can be effectively affected by changing the physical parameters (including the distribution type and the mass fraction of GPLs). UD and FG-A have the maximum and minimum resonance frequencies respectively, and under the FG-A distribution type, the snap-bucking phenomenon of curved beam is the most obvious. With the increase of GPLs mass fraction, the dynamic and static behaviors of curved beams become more and more obvious. When g=0, the curved beams resonate first and the buckling strength is the minimum. With the increase of the mass fraction of GPLs, the resonance position is delayed and the buckling strength is increasing.

(3) As the number of GPLs layers increase, resonant frequency and buckling strength of C-H and H-H curved beams increase. When N=12, there is the maximum resonance position and the most obvious snap-buckling phenomenon.

(4) When there is no elastic foundation, C-H and H-H curved beams have the maximum buckling strength and the minimum resonance position. And with the increase of elastic foundation, the buckling strength slowly decreases and the resonance position becomes larger. In addition, C-H curved beam behaves as hard-springs with or without elastic foundations. However, for H-H curved beam, with the increases of elastic

foundation, H-H curved beam will change from soft-springs to hard-springs

References

Abumandour, R.M., El-Shorbagy, M.A., Eldesoky, I.M., Kamel, M.H., Alotaibi, H. and Felila, A.L. (2022), "Deflection analysis of a nonlocal euler-bernoulli nanobeam model resting on two elastic foundations: A generalized differential quadrature approach", *Symmetry-basel*, **14**(11), 2342. https://doi.org/10.3390/sym14112342.

Al-Furjan, M.S.H., Yin, C., Shen, X., Kolahchi, R., Zarei, M.S. and Hajmohammad, M.H. (2022), "Energy absorption and vibration of smart auxetic FG porous curved conical panels resting on the frictional viscoelastic torsional substrate", *Mech. Syst. Signal. Pr.*, **178**, 109269. https://doi.org/10.1016/j.ymssp.2022.109269.

Alazwari, M.A., Daikh, A.A., Houari, M.S., Tounsi, A. and Eltaher, M.A. (2021), "On static buckling of multilayered carbon nanotubes reinforced composite nanobeams supported on non-linear elastic foundations", *Steel. Compos. Struct.*, **40**(3), 389-404. https://doi.org/10.12989/scs.2021.40.3.389.

Amir, M., Kim, S.W. and Talha, M. (2022), "On the stochastic vibration analysis of the geometrically nonlinear graded cellular curved panels with material stochasticity", *Int. J. Pres. Ves. Pip.*, **199**, 104768. https://doi.org/10.1016/j.ijpvp.2022.104768.

Assie, A.E., Mohamed, S.A., Shanab, R.A., Abo-bakr, R.M. and Eltaher, M.A. (2023), "Static buckling of 2D FG porous plates resting on elastic foundation based on unified shear theories", *J. Appl. Comput. Mech.*, **9**(1), 239-258. https://doi.org/10.22055/jacm.2022.41265.3723.

Babaei, H. (2021), "On frequency response of FG-CNT reinforced composite pipes in thermally pre/post buckled configurations", *Compos. Struct.*, 276, 114467. https://doi.org/10.1016/j.compstruct.2021.114467.

Babaei, H. (2022a), "Nonlinear analysis of size-dependent frequencies in porous FG curved nanotubes based on nonlocal strain gradient theory", *Eng. Struct.*, **38**, 1717-1734. https://doi.org/10.1007/s00366-021-01317-7.

Babaei, H. (2022b), "Free vibration and snap-through instability of FG-CNTRC shallow arches supported on nonlinear elastic foundation", *Appl. Math. Comput.*, **413**, 126606. https://doi.org/10.1016/j.amc.2021.126606.

Babaei, H. and Eslami, M.R. (2021a), "Nonlinear analysis of thermal-mechanical coupling bending of FGP infinite length cylindrical panels based on PNS and NSGT", *Appl. Math. Model.*, **91**, 1061-1080. https://doi.org/10.1016/j.apm.2020.10.004

Babaei, H. and Eslami, M.R. (2021b), "Nonlinear analysis of thermal-mechanical coupling bending of clamped FG porous curved micro-tubes", *J. Therm. Stresses*, **44**(4), 409-432. https://doi.org/10.1080/01495739.2020.1870417.

Babaei, H., Kiani, Y. and Eslami, M.R. (2018a), "Geometrically nonlinear analysis of functionally graded shallow curved tubes in thermal environment", *Thin-Walled Struct.*, **132**, 48-57. https://doi.org/10.1016/j.tws.2018.08.008.

Babaei, H., Kiani, Y. and Eslami, M.R. (2018b), "Geometrically nonlinear analysis of shear deformable FGM shallow pinned arches on nonlinear elastic foundation under mechanical and thermal loads", *Acta. Mech.*, **229**(7), 3123-3141. https://doi.org/10.1007/s00707-018-2134-2.

Babaei, H., Kiani, Y. and Eslami, M.R. (2018c), "Application of two-steps perturbation technique to geometrically nonlinear analysis of long FGM cylindrical panels on elastic foundation under thermal load", *J. Therm, Stress.*, **41**(7), 847-865. https://doi.org/10.1080/01495739.2017.1421054.

Babaei, H., Kiani, Y. and Eslami, M.R. (2019a), "Thermal buckling and post-buckling analysis of geometrically imperfect FGM clamped tubes on nonlinear elastic foundation", *Appl. Math. Model.*, **71**, 12-30. https://doi.org/10.1016/j.apm.2019.02.009.

Babaei, H., Kiani, Y. and Eslami, M.R. (2019b), "Large amplitude free vibration analysis of shear deformable FGM shallow arches on nonlinear elastic foundation", *Thin-Walled Struct.*, **144**, 48-57. https://doi.org/10.1016/j.tws.2019.106237.

Babaei, H., Kiani, Y. and Eslami, M.R. (2019c), "Large amplitude free vibrations of long FGM cylindrical panels on nonlinear elastic foundation based on physical neutral surface", *Compos. Struct.*, **220**, 888-898. https://doi.org/10.1016/j.compstruct.2019.03.064.

Babaei, H., Kiani, Y. and Eslami, M.R. (2019d), "Buckling and post-buckling analysis of geometrically imperfect FGM pin-ended tubes surrounded by nonlinear elastic medium under compressive and thermal loads", *Int. J. Mech. Mater. Des.*, **15**(2), 225-244. https://doi.org/10.1007/s10999-018-9420-y.

Babaei, H., Kiani, Y. and Eslami, M.R. (2019e), "Thermomechanical nonlinear in-plane analysis of fix-ended FGM shallow arches on nonlinear elastic foundation using two-step perturbation technique", *Int. J Struct. Stab. Dynam.*, **19**(8), 1950089. https://doi.org/10.1142/S0219455419500895.

Basha, M., Daikh, A.A., Melaibari, A., Wagih, A., Othman, R., Almitani, K.H., Hamed, M.A., Abdelrahman, A. and Eltaher, M.A. (2022), "Nonlocal strain gradient theory for buckling and bending of FG-GRNC laminated sandwich plates", *Steel. Compos. Struct.*, **43**(5), 639-660. https://doi.org/10.12989/scs.2022.43.5.639.

Chaabani, H., Mesmoudi, S., Boutahar, L. and El Bikri, K. (2022), "Buckling of porous FG sandwich plates subjected to various non-uniform compressions and resting on Winkler-Pasternak elastic foundation using a finite element model based on the high-order shear deformation theory", *Acta. Mech.*, **233**(12), 5359-5376. https://doi.org/10.1007/s00707-022-03388-z.

Chen, J.S., Wen, Q.W. and Yeh, C. (2022), "Steady state responses of an infinite beam resting on a tensionless visco-elastic foundation under a harmonic moving load", *J. Sound. Vib.*, **540**, 17298. https://doi.org/10.1016/j.jsv.2022.117298.

Chen, R., Wang, W., Wu, K., Zheng, G., Xu, X.J., Wang, H.G. and Luo, J. (2023), "Design and optimization of a novel compliant planar parallelogram mechanism utilizing initially curved beams", *Mech. Mach. Theory.*, **179**, 105092. https://doi.org/10.1016/j.mechmachtheory.2022.105092.

Chen, X., Zhao, J.L., She, G.L., Jing, Y., Luo, J. and Pu, H.Y. (2022a), "On wave propagation of functionally graded CNT strengthened fluid-conveying pipe in thermal environment", *Eur. Phys. J. Plus.*, **137**(10), 1158. https://doi.org/10.1140/epjp/s13360-022-03234-0.

Chen, X., Zhao, J.L., She, G.L., Jing, Y., Pu, H.Y. and Luo, J. (2022b), "Nonlinear free vibration analysis of functionally graded carbon nanotube reinforced fluid-conveying pipe in thermal environment", *Steel. Compos. Struct.*, **45**(5), 641-652. https://doi.org/10.12989/scs.2022.45.5.641.

Chinnapandi, L.B.M., Pitchaimani, J. and Eltaher, M.A. (2022), "Vibro-acoustics of functionally graded porous beams subjected to thermo-mechanical loads", *Steel. Compos. Struct.*, **44**(6), 815-829. https://doi.org/10.12989/scs.2022.44.6.815.

Daikh, A.A., Belarbi, M.O., Ahmed, D., Houari, M.S.A., Avcar, M., Tounsi, A., and Eltaher, M.A. (2022), "Static analysis of functionally graded plate structures resting on variable elastic foundation under various boundary conditions", *Acta. Mech.*, https://doi.org/10.1007/s00707-022-03405-1.

Deng, L.F., Niu, M.Q., Xue, J. and Chen, L.Q. (2023), "An ALE formulation for the geometric nonlinear dynamic analysis of planar curved beams subjected to moving loads", *Mech. Syst. Signal. Pr.*, **184**, 109670. https://doi.org/10.1016/j.ymssp.2022.109670.

Ding, H.X. and She, G.L. (2021), "A higher-order beam model for the snap-buckling analysis of FG pipes conveying fluid", *Struct. Eng. Mech.*, **80**(1), 63-72.

https://doi.org/10.12989/sem.2021.80.1.063.
Ding, H.X., She, G.L. and Zhang, Y.W. (2022a), "Nonlinear buckling and resonances of functionally graded fluid-conveying pipes with initial geometric imperfection", *Eur. Phys. J. Plus*, **137**,1329. https://doi.org/10.1140/epjp/s13360-022-03570-1.
Ding, H.X., Zhang, Y.W. and She, G.L. (2022b), "On the resonance problems in FG-GPLRC beams with different boundary conditions resting on elastic foundations", *Comput. Concrete*, **30**(6), 433-443. https://doi.org/10.12989/cac.2022.30.6.433.
Eltaher, M.A., Mohamed, N., Mohamed, S.A. and Seddek, L.F. (2019), "Periodic and nonperiodic modes of postbuckling and nonlinear vibration of beams attached to nonlinear foundations", *Appl. Math. Model*., **75**, 414-445. https://doi.org/10.1016/j.apm.2019.05.026.
Ermis, M., Kutlu, A., Eratli, N. and Omurtag, M.H. (2022), "Free vibration of axially FG curved beam on orthotropic Pasternak foundation via mixed FEM", *J. Braz. Soc. Mech. Sci*., **44**(12), 597. https://doi.org/10.1007/s40430-022-03853-9.
Esmaeili, H.R., and Kiani, Y. (2022), "Vibrations of graphene platelet reinforced composite doubly curved shells subjected to thermal shock", *Mech. Based. Des. Struct*., https://doi.org/10.1080/15397734.2022.2120499.
Gao, Y., Xiao, W.S. and Zhu, H.P. (2020), "Snap-buckling of functionally graded multilayer graphene platelet-reinforced composite curved nanobeams with geometrical imperfections", *Eur. J. Mech. A-Solid*., **82**, 103993. https://doi.org/10.1016/j.euromechsol.2020.103993.
Hendi, A., Eltaher, M.A, Mohamed, S.A. and Attia, M. (2022), "Nonlinear thermal vibration of pre/post-buckled two-dimensional FGM tapered microbeams based on a higher order shear deformation theory", *Steel Compos. Struct*., **41**(6), 787-802. http://doi.org/DOI10.12989/scs.2021.41.6.787.
Homaeinezhad, M.R. and Gavari, M.A. (2022), "Feedback control of actuation-constrained moving structure carrying Timoshenko beam", *Int. J. Robust. Nonlin*., https://doi.org/10.1002/rnc.6471.
Hu, S.W., Zhong, R., Wang, Q.S., Qin, B., and Shao, W. (2022), "A strong-form Chebyshev-RPIM meshless solution for free vibration of conical shell panels with variable thickness and fiber curvature", *Compos. Struct*., **296**, 115884. https://doi.org/10.1016/j.compstruct.2022.115884.
Huang, W.C., Qin, L.H. and Chen, Q. (2022), "Numerical exploration on snap buckling of a pre-stressed hemispherical gridshell", *J. Appl. Mech -T. ASME*., **89**(1), 011005. https://doi.org/10.1115/1.4052289.
Jiang, Y.L., Sun, H.Y. and Yan, H.J. (2022), "Vibration-impact study on the functionally graded graphene nanoplatelets reinforced composite curved open-type shell", *Wave. Random. Complex*, https://doi.org/10.1080/17455030.2022.2117875
Kallannavar, V. and Kattimani, S. (2023), "Effect of temperature and porosity on free vibration characteristics of a doubly-curved skew laminated sandwich composite structures with 3D printed PLA core", *Thin. Wall. Struct*., **182**, 110263. https://doi.org/10.1016/j.tws.2022.110263.
Li, C., Shen, H.S. and Yang, J. (2022), "Design and nonlinear dynamics of FG curved sandwich beams with self-adapted auxetic 3D double-V meta-lattice core", *Eng. Struct*., **272**, 115023. https://doi.org/10.1016/j.engstruct.2022.115023.
Lu, L., She, G.L. and Guo, X. (2021), "Size-dependent postbuckling analysis of graphene reinforced composite microtubes with geometrical imperfection", *Int. J. Mech. Sci*., **199**, 106428. https://doi.org/10.1016/j.ijmecsci.2021.
Malikan, M., Tornabene, F. and Dimitri, R. (2019), "Transient response of oscillated carbon nanotubes with an internal and external damping", *Compos. Part B: Eng*., **158**, 198-205. https://doi.org/10.1016/j.compositesb.2018.09.092.
Malikan, M., Wiczenbach, T. and Eremeyev, V.A. (2022), "Thermal buckling of functionally graded piezomagnetic micro-and nanobeams presenting the flexomagnetic effect", *Continuum Mech. Thermodynam*., **34**(4), 1051-1066. https://doi.org/10.1007/s00161-021-01038-8.
Melaibari, A., Mohamed, S.A., Assie, A.E., Shanab, R.A. and Eltaher, M.A. (2023), "Static response of 2D FG porous plates resting on elastic foundation using midplane and neutral surfaces with movable constraints", *Mathematics*, **10**(24), 4784. https://doi.org/10.3390/math10244784.
Melchiorre, J., Manuello, A., Marmo, F., Adriaenssens, S. and Marano, G.C. (2023), "Differential formulation and numerical solution for elastic arches with variable curvature and tapered cross-sections", *Eur. J. Mech. A-Solid*, **97**, 104757. https://doi.org/10.1016/j.euromechsol.2022.104757.
Mohamed, N., Mohamed, S.A. and Eltaher, M.A. (2021), "Buckling and post-buckling behaviors of higher order carbon nanotubes using energy-equivalent model", *Eng. with Comput*., **37**(4), 2823-2836. http://dx.doi.org/10.1007/s00366-020-00976-2.
Mohamed, S.A., Mohamed, N. and Eltaher, M.A. (2022), "Snap-through instability of helicoidal composite imperfect beams surrounded by nonlinear elastic foundation", *Ocean. Eng*., **263**, 112171. https://doi.org/10.1016/j.oceaneng.2022.112171.
Pham, H.A., Tran, H.Q., Tran, M.T., Nguyen, V. and Huong, Q.T. (2022), "Free vibration analysis and optimization of doubly-curved stiffened sandwich shells with functionally graded skins and auxetic honeycomb core layer", *Thin. Wall. Struct*., **179**, 109571. https://doi.org/10.1016/j.tws.2022.109571.
Pham, Q.H., Tran, V.K. and Nguyen, P.C. (2022), "Hygro-thermal vibration of bidirectional functionally graded porous curved beams on variable elastic foundation using generalized finite element method", *Case. Stud. Therm. Eng*., **40**, 102478. https://doi.org/10.1016/j.csite.2022.102478.
Pham, Q.H., Tran, V.K., Tran, T.T., Nguyen, P.C. and Malekzadeh, P. (2022), "Dynamic instability of magnetically embedded functionally graded porous nanobeams using the strain gradient theory", *Alex. Eng. J.*, **61**(12), 10025-10044. https://doi.org/10.1016/j.aej.2022.03.007.
Qiao, W.Z., Guo, T.D., Kang, H.J. and Zhao, Y.Y. (2022), "An asymptotic study of nonlinear coupled vibration of arch-foundation structural system", *Eur. J. Mech. A-Solid*., **96**, 104711. https://doi.org/10.1016/j.euromechsol.2022.104711.
Shahmohammadi, M.A., Mirfatah, S.M., Salehipour, H. and Civalek, O. (2023), "On nonlinear forced vibration of micro scaled panels", *Int. J. Eng. Sci*., **182**, 103774. https://doi.org/10.1016/j.ijengsci.2022.103774.
She, G.L. (2020), "Wave propagation of FG polymer composite nanoplates reinforced with GNPs", *Steel Compos. Struct*., **37**(1) , 27-35. https://doi.org/10.12989/scs.2020.37.1.027.
She, G.L. (2021), "Guided wave propagation of porous functionally graded plates: The effect of thermal loadings", *J. Therm. Stresses*, **44**(10), 1289-1305. https://doi.org/10.1080/01495739.2021.1974323.
She, G.L. and Ding, H.X. (2023), "Nonlinear primary resonance analysis of initially stressed graphene platelet reinforced metal foams doubly curved shells with geometric imperfection", *Acta Mech. Sin*., **39**, 522392. https://doi.org/10.1007/s10409-022-22392-x.
She, G.L. and Li, Y.P. (2022), "Wave propagation in an FG circular plate in thermal environment", *Geomech. Eng*., **31**(6), 615-622. https://doi.org/10.12989/gae.2022.31.6.615.
She, G.L., Ding, H.X. and Zhang, Y.W. (2022), "Wave propagation in a FG circular plate via the physical neutral surface concept", *Struct. Eng. Mech*., **82**(2), 225-232. https://doi.org/10.12989/sem.2022.82.2.225.
She, G.L., Liu, H.B. and Karami, B. (2021), "Resonance analysis of composite curved microbeams reinforced with graphene nanoplatelets", *Thin Wall. Struct*., **160**, 107407. https://doi.org/10.1016/j.tws.2020.107407

Tornabene, F., Viscoti, M. and Dimitri, R. (2022), "Higher order theories for the free vibration analysis of laminated anisotropic doubly-curved shells of arbitrary geometry with general boundary conditions", *Compos. Struct*., **297**, 115740. https://doi.org/10.1016/j.compstruct.2022.115740.

Tornabene, F., Viscoti, M. and Dimitri, R. (2023), "Static analysis of anisotropic doubly-curved shell subjected to concentrated loads employing higher order layer-wise theories", *Cmes -Comp. Model. Eng*., **134**(2), 1393-1468. https://doi.org/10.32604/cmes.2022.022237.

Tung, H.V. (2018), "Nonlinear thermomechanical response of pressure-loaded doubly curved functionally graded material sandwich panels in thermal environments including tangential edge constraints", *J. Sandw. Struct. Mater*., **20**(8), 974-1008. https://doi.org/10.1177/1099636216684312.

Van Long, N., Thinh, T.I., Bich, D.H. and Tu, T.M. (2022), "Nonlinear dynamic responses of sandwich-FGM doubly curved shallow shells subjected to underwater explosions using first-order shear deformation theory", *Ocean. Eng*., **260**, 111886. https://doi.org/10.1016/j.oceaneng.2022.111886.

Wang, X.S., Wu, S.B., Yin, J.M., Moradi, Z., Safa, M. and Khadimallah, M.A. (2023), "On the electromechanical energy absorption of the reinforced composites piezoelectric MEMS via Adaptive neuro-fuzzy inference system and MCS theory", *Compos. Struct*., **303**, 116246. https://doi.org/10.1016/j.compstruct.2022.116246.

Xiong, Z.H., Kou, L., Zhao, J.J., Cui, H. and Wang, B. (2022), "Isogeometric analysis of longitudinal displacement of a simplified tunnel model based on elastic foundation beam", *Cmes-Comp. Model. Eng*. https://doi.org/10.32604/cmes.2023.024833.

Xu, J.Q. and She, G.L. (2022), "Thermal post-buckling analysis of porous functionally graded pipes with initial geometric imperfection", *Geomech. Eng*., **31**(3), 329-337. https://doi.org/10.12989/gae.2022.31.3.329.

Zhai, Y.J., Ma, Z.S., Ding, Q. and Wang, X.P. (2023), "Nonlinear transverse vibrations of a jointed structure with two slightly curved beams connected by complex elastic joints", *Int. J. Nonlin. Mech*., **148**, 104259. https://doi.org/10.1016/j.ijnonlinmec.2022.104259.

Zhang, Y.W. and She, G.L. (2022), "Wave propagation and vibration of FG pipes conveying hot fluid", *Steel. Compos, Struct*., **42**(3) 397-405. https://doi.org/10.12989/scs.2022.42.3.397.

Zhang, Y.W. and She, G.L. (2023a), "Nonlinear low-velocity impact response of graphene platelet-reinforced metal foam cylindrical shells under axial motion with geometrical imperfection", *Nonlinear Dynam*., https://doi.org/10.1007/s11071-022-08186-9.

Zhang, Y.W. and She, G.L. (2023b), "Nonlinear primary resonance of axially moving functionally graded cylindrical shells in thermal environment", *Mech. Adv. Mater. Struct*., https://doi.org/10.1080/15376494.2023.2180556.

Zhang, Y.W., Ding, H.X. and She, G.L. (2022), "Snap-buckling and resonance of functionally graded graphene reinforced composites curved beams resting on elastic foundations in thermal environment", *J. Therm. Stresses*, **45**(12), 1029-1042. https://doi.org/10.1080/01495739.2022.2125137.

Zhang, Y.W., Ding, H.X. and She, G.L. (2023a), "Wave propagation in spherical and cylindrical panels reinforced with carbon nanotubes", *Steel Compos. Struct*., **46**(1), 133-141. https://doi.org/10.12989/scs.2023.46.1.133.

Zhang, Y.W., She, G.L. and Ding, H.X. (2023b), "Nonlinear resonance of graphene platelets reinforced metal foams plates under axial motion with geometric imperfections", *Eur. J. Mech. A-Solid*., **98**, 104887. https://doi.org/10.1016/j.euromechsol.2022.104887.

Zhang, Y.Y., Wang, X.Y., Zhang, X., Shen, H.M. and She, G.L. (2021), "On snap-buckling of FG-CNTRC curved nanobeams considering surface effects", *Steel Compos. Struct*., **38**(3), 293-304. https://doi.org/10.12989/scs.2021.38.3.293.

Zhao, J.L., Chen, X., She, G.L., Jing, Y., Bai, R.Q., Yi, J., Pu, H.Y. and Luo, J. (2022a), "Vibration characteristics of functionally graded carbon nanotube-reinforced composite double-beams in thermal environments", *Steel. Compos. Struct*., **43**(6), 797-808. https://doi.org/10.12989/scs.2022.43.6.797.

Zhao, J.L., She, G.L., Wu, F., Yuan, S.J., Bai, R.Q., Pu, H.Y., Wang, S.L. and Luo, J. (2022b), "Guided waves of porous FG nanoplates with four edges clamped", *Adv. Nano. Res*., **13**(5), 465-474. https://10.12989/anr.2022.13.5.465.

CC